Chapter 1

Graphene Thin Films and Graphene Decorated with Metal Nanoparticles

Paul Bazylewski, Arash Akbari-Sharbaf, Sabastine Ezugwu, Tianhao Ouyang, Jaewoo Park and Giovanni Fanchini

Additional information is available at the end of the chapter

http://dx.doi.org/10.5772/63279

Abstract

The electronic, thermal, and optical properties of graphene-based materials depend strongly on the fabrication method used and can be further manipulated through the use of metal nanoparticles deposited on the graphene surface. Metals that strongly interact with graphene such as Co and Ni can form strong chemical bonds which may significantly alter the band structure of graphene near the Dirac point. Weakly interacting metals such as Au and Cu can be used to induce shifts in the graphene Fermi energy, resulting in doping without significant alteration to the graphene band structure. The deposition and nucleation conditions such as deposition rate, annealing temperature and time, and annealing atmosphere can be used to control the size and distribution of metal nanoparticles. Under ideal conditions, self-assembled arrays of nanoparticles can be obtained on graphene-based films for use in new types of nanodevices such as evanescent waveguides.

Keywords: graphene, thin films, metal nanoparticles, optical properties, electronic band structure

1. Introduction

Graphene is a single layer of carbon atoms bonded in a hexagonal honeycomb lattice, resulting in a structure with many desirable characteristics that are attractive for several applica-

tions. These unique properties include high charge carrier mobility and thermal conductivity, coupled with a large surface area that is ideal for catalysis or sensing applications. However, utilizing graphene effectively in many technological applications depends on fabrication of the appropriate type of graphene-based material ranging from large area single and few-layer graphene sheets to laminate films sintered from many nano- or micro-meter-sized graphene platelets.

High-quality single- and few-layer graphene up to a thickness of ~10 layers can be successfully fabricated using vacuum-based deposition technologies such as chemical vapor deposition (CVD) [1]. CVD graphene can be grown on metal substrates that are lattice matched to the graphene lattice such as Ni(111) and Cu, using a carrier gas usually composed of CH_4 that reacts with the surface under high-temperature conditions to promote graphene growth. Both substrate types can be used to produce high-quality single- and few-layer graphene using CVD, although the specific growth method varies depending on the substrate material. Graphene grown by CVD methods has been shown to have excellent electronic properties and can closely approximate the predicted theoretical performance of graphene sheets. However, high-quality graphene grown by CVD can be costly to produce and is sensitive to contamination and defects, making it difficult to utilize effectively in many device applications. Since the substrates used in graphene growth is not desirable for all device architectures, the graphene must be transferred to another substrate such as Si/SiO_2. This is commonly accomplished using a solution-based method utilizing a sacrificial polymer such as poly-methyl-methacrylate (PMMA) or another cross-linked polymer, but can introduce defects and contamination [1, 2].

To overcome these difficulties, solution-based methods that do not utilize vacuum systems have been developed. These methods concentrate on chemical exfoliation of graphite to produce colloidal dispersions of few-layer graphene platelets. This approach produces an oxidized form of graphene known as graphene oxide (GO) that is dispersible in aqueous solutions due to intercalation of oxygen functional groups within the graphite lattice. This approach is scalable and versatile in terms of chemical functionalization and use with a variety of substrates. However, one significant disadvantage of colloidal dispersions is films of GO are highly insulating due to a high density of oxygen functional groups, and must be reduced in order to recover the desirable properties of graphene [3]. This can be accomplished using chemical reductants or thermal treatment to remove oxygen and restore conductivity. However, the reduction process is intrinsically energetic and unavoidably results in defects in the graphene lattice that negatively impact the electronic properties of the final graphene film.

Recent advances in solution processing of graphite have been focussed on limiting the use of strong acid treatments to control the oxidation, and instead make use of surfactants to aid the exfoliation process. Ribonucleic acid (RNA) has been used by Sharifi *et al*. [4] as an effective aqueous surfactant to exfoliate graphite that is weakly oxidized in comparison to GO before reduction. Weakly oxidized graphene of this type has been shown to be dispersible in water due to RNA absorption (**Figure 1**) and is conductive as-deposited from solution without further treatment to remove oxygen functional groups.

http://dx.doi.org/10.5772/63279

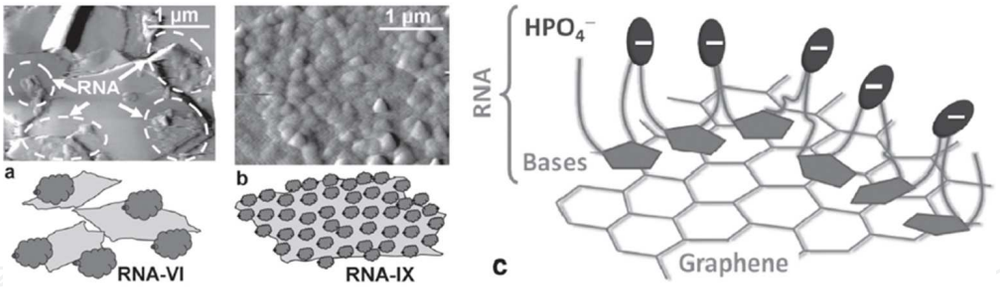

Figure 1. (a, b) Atomic force microscopy phase images demonstrating the arrangement of two types of RNA, RNA VI, and IX aggregates on specific surface regions of small exfoliated graphene flakes. (c) The adhesion mechanism of RNA where a combination of hydrophobic bases and hydrophilic phosphate groups keep the graphene-RNA suspended in water. Reproduced with permission from Ref. [4].

Both types of graphene from either vacuum-based or solution-based fabrication can be utilized as active layers in thin-film electronic devices, or further modified using metal nanoparticles. Doping effects from metal nanoparticles may be used to shift the graphene work function for solar cell applications or light-emitting diode (LED) applications. Organized nanostructures such as self-assembled ordered superlattices of metal nanoparticles can be used as plasmonic waveguides [5, 6]. The electronic band structure of graphene can be altered by applying metallic layers on its surface, where this effect is strongly dependent on the specific type of metal being used. A strong interaction from the formation of strong chemical bonds with metals, such as Co, Ni, and Pd, may significantly alter the band structure of graphene near the Dirac point. For weakly bonding metals (Cu, Al, Ag, Au, and Pt), shifts in the graphene Fermi energy can be induced due to electron transfer, resulting in doping without significant alteration to the graphene band structure.

2. Research and methods

2.1. Graphene thin film fabrication

The use of vacuum techniques to fabricate high-quality large area sheets of single-layer graphene is of great interest for device applications and the study of the fundamental physics of graphene. Metal substrates most commonly used are Ni and Cu because they possess a crystal structure with a lattice spacing well matched to that of graphene. Ni(111) is ideal for graphene growth as it possesses a lattice structure reminiscent of the hexagonal lattice of graphene with similar lattice constants. Graphene is fabricated starting on a polycrystalline Ni substrate that is first annealed in an Ar/H_2 atmosphere at high temperature (800–1000°C) to increase the grain size. A polycrystalline substrate is lower in cost than a single crystal, but intrinsically contains grain boundaries that limit the maximum size of graphene grains. The heated Ni substrate is then exposed to a H_2/CH_4 gas mixture. Upon contact with the Ni, the hydrocarbons decompose and carbon atoms dissolve into the Ni film, forming a solid solution. Cooling of the sample with argon gas causes carbon atoms to diffuse out from the Ni-C solid solution and precipitate on the Ni surface in the form of graphene films. The use of Cu as a substrate is a similar process involving the same carrier gases; however, carbon has a much

lower solubility in Cu at elevated temperature than Ni. Since Cu is also well lattice matched to graphene, rather than dissolving, the hydrocarbons decompose on the surface of Cu into a graphene layer [1]. This technique can produce multilayer graphene easily by simply allowing the reaction to proceed for a longer length of time to build up a graphene multilayer. CVD graphene on Cu or Ni can be transferred to other substrates to become part of device architecture or used for further processing with metal nanoparticles or chemical functionalization.

This procedure is advantageous for applications that require single- or few-layer graphene. CVD films are highly transparent (98% transparency to visible light) and conductive (100–1000 Ω/square), making them ideal as a potential replacement for more expensive transparent conducting materials such as indium tin oxide (ITO) in solar cell devices. However, the need for a large, single-crystal substrate limits the ultimate size of a single-grain graphene sheet. The solution transfer process used to integrate CVD graphene into devices further limits the use of CVD graphene by introducing defects and a PMMA residue that is difficult to sufficiently remove. These factors limit the ultimate size of defect-free graphene grains that can be obtained using a CVD graphene fabrication process.

Alternative to vacuum-based techniques, the methods based on chemical exfoliation of graphite can be used to obtain colloidal suspensions of graphene in aqueous or solvent solution. This approach is scalable, has the potential for high-volume production, and is versatile in terms of chemical functionalization. Graphite oxide has been mainly produced by one of three common methods, the Brodie, Staudenmaier, or Hummers methods, which all utilize the oxidation of graphite in the presence of strong acids and oxidants [2]. Brodie and Staudenmaier use a combination of potassium chlorate ($KClO_3$) with nitric acid (HNO_3) to oxidize graphite, and Hummers treats the graphite with potassium permanganate ($KMnO_4$) and sulfuric acid (H_2SO_4). The level of oxidation can be varied on the basis of the specific method and reaction conditions, and the precursor graphite material used. Graphite oxide consists of a layered structure of graphene oxide sheets that are strongly hydrophilic due to an excess of oxygen functional groups such that intercalation of water molecules between the layers readily occurs.

Colloidal solutions of GO can be used to produce laminate films formed of graphene platelets using a variety of methods to separate GO platelets from solution such as vacuum filtration, dip coating, spin coating, or Langmuir-Blodgett film assembly [3]. However, the use of GO directly produces insulating films that must be reduced to remove a fraction of oxygen functional groups and restore conductivity. Several methods exist to reduce GO including chemical reduction using reducing agents such as hydrazine or hydroquinone, thermal annealing, or ultraviolet-assisted reduction. Although successful to reduce GO, defects are unavoidably introduced in the graphene lattice after reduction. Defects act to reduce the electrical and thermal conductivity of reduced GO and can also spread to unzip large GO sheets into smaller domains. Alternative methods exist to produce graphene suspensions using only weak oxidation of graphite combined with another material to behave as a surfactant and promote dispersion in water. Surfactants such as sodium dodecylbenzene sulfonate (SDBS) can be used to enhance graphite exfoliation without the use of strong oxidation treatments to saturate the graphite layers with oxygen functional groups and promote water solubility. RNA

has been used as a low cost and biocompatible surfactant to disperse weakly oxidized graphite in water [4]. The use of an additional material to aid in exfoliation allows the graphite to be dispersed in water without being strongly oxidized, and therefore does not require reduction to become conductive.

2.2. Electrical and thermal properties of graphene thin films

Graphene thin films formed from interlocking and overlapping platelets of graphene or GO have electrical, optical, and thermal properties that diverge from those of single-layer graphene. A single layer of graphene has optical transparency of approximately 98%, which decreases as the number of layers increases. The electrical conductivity of few-layer graphene is typically lower than a multilayer, providing a trade-off of increased conductivity for lower transparency. Multilayer graphene laminates, therefore, have lower optical transparency compared to single-layer graphene, but can have much lower resistivity approaching 100–1000 Ω/square.

Graphene and graphene-based thin films, however, are superior to ITO for thermal management applications since the thermal conductivity of ITO is relatively low (5.9 W m^{-1} K^{-1}) compared to graphene laminate films (~10^2 W m^{-1} K^{-1}) [7]. Interestingly, the excellent thermal properties of single-layer graphene are also retained to a large extent in thin graphite multilayers and graphene laminate films. In ITO, the thermal properties at room temperature conditions are determined primarily by the electronic band structure. By contrast, thermal characteristics in graphene-based materials require a more complex interpretation due to important effects from lattice vibrations [7]. The thermal and electrical conductivity of graphene-based thin films strongly depend on the average number of graphene layers forming the platelets, their lateral size, and density of the flakes including voids between neighboring domains [8, 9].

Electrical conductivity of graphene-based films is greatly affected by both the preparation method and the post-treatments. Graphene-based films produced using RNA as a surfactant reveal a trend of decreasing sheet resistance with annealing temperature from Sharifi *et al*. shown in **Figure 2** [4]. The decrease in sheet resistance as a function of the annealing temperature demonstrates that annealing is effective in improving the conductivity of RNA-surfactant-based films without altering transparency. RNA is insulating and tends to decompose above room temperature; the amount of RNA aggregates intercalating the graphene flakes decreases dramatically upon annealing at high temperature (510°C), leading to better conduction between flakes and improved overall conductivity. The effect of thermal annealing is compared to functionalization where the sheet resistance decreased after initial exposure to a nitric acid (HNO_3) bath, followed by a further decrease after soaking in thionyl chloride ($SOCl_2$) without a decrease in transparency. This combination of treatments leads to thin films with sheet resistance of 200 Ω/square at 50% transmittance, or 2.3 MΩ/square at 85% transmittance. Although this performance is inferior to graphene materials epitaxially grown on copper, it is comparable to other classes of graphene-based thin films such as SDBS-based graphene dispersions.

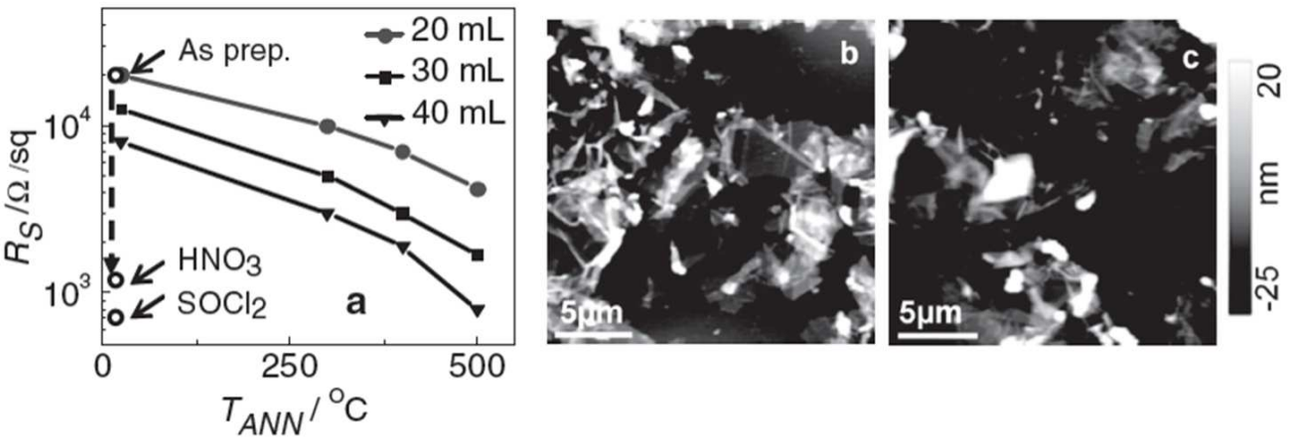

Figure 2. (a) Sheet resistance as a function of annealing temperature for graphene-RNA VI films at different filtration volumes. (b) AFM image before annealing. (c) AFM image of the same sample after annealing. Reproduced with permission from Ref. [4].

2.3. Graphene thin films decorated with metal nanoparticles

Graphene-based film properties can be altered through the use of metal nanoparticles (NPs) applied to the surface. Introducing metal nanoparticles to graphene has been used to shift the work function of graphene, open a band gap, and produce ordered nanostructure super lattices depending on the strength of metal-graphene interaction. For strongly interacting metals, the graphene-metal separation depends on the available bonding locations where the graphene has the appropriate position with respect to the substrate such that bonding can be optimized and the separation is minimized.

Gold nanoparticles are an example of weakly interacting metal particles that can be used to induce plasmonic effects that are useful in applications such as plasmonic solar cells and optical memory devices. Venter *et al*. [10] used graphene thin films obtained from RNA-surfactant-assisted exfoliation of graphite as a substrate that was coated with Au_{144} NP clusters using spin coating from a toluene solution containing $Au_{144}(SCH_2CH_2Ph)_{60}$ molecules synthesized using a modified Brust-Schiffrin method. SEM images of nucleated Au NPs are shown in **Figure 3**. A post-annealing step is used to promote nucleation of Au_{144} into NPs and also releases the capping ligands of Au_{144} molecules, similar to what has been observed for the nucleation of Au_{25} molecular nanoclusters and the expulsion of the corresponding ligands with the formation of Au NPs in polymers [11]. Pre-annealing was also utilized to decompose the RNA and remove it from the film, leaving defects and impurity on the graphene surface that may act as nucleation sites for Au_{144} to aggregate and form NPs when annealed. Similar deposition on graphene-based films using SDBS did not show nucleation of nanoparticles, indicating RNA plays a crucial role in Au NP nucleation. Metal nanoparticles nucleated in this way are advantageous because a uniform layer of Au NPs is formed with a size independent of the number of graphene layers, in contrast to traditional methods of annealing colloidal or thermally evaporated gold thin films which have a size and morphology dependent on the number of graphene layers beneath.

http://dx.doi.org/10.5772/63279

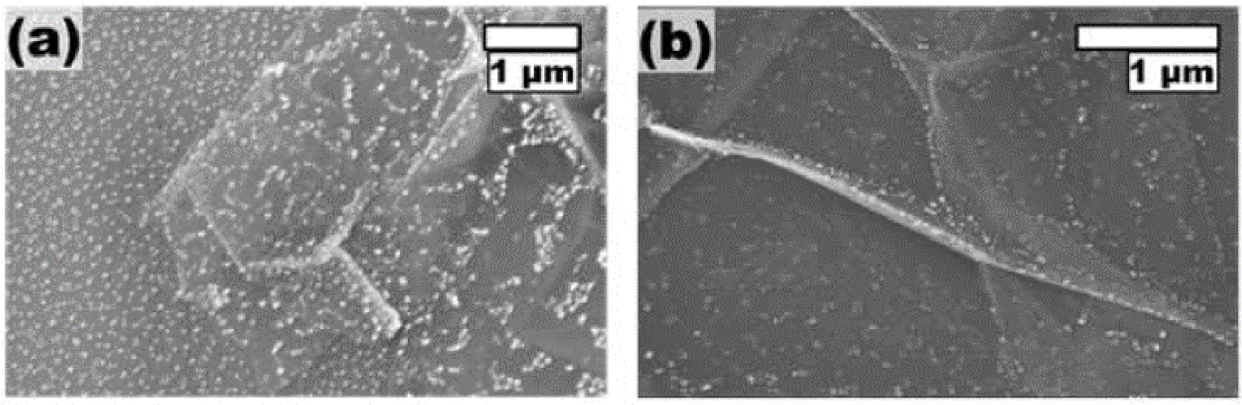

Figure 3. SEM images of graphene thin films deposited on glass decorated with Au NPs. Pre-annealing of the substrate at 300°C for 20 min was combined with 200°C heating for 30 min after Au deposition to nucleate Au-NPs. (a) Au-NPs spin coated at 3000 rpm for 60 s. (b) Au-NPs spin coated at 4000 rpm for 60 s. Reproduced with permission from Ref. [10].

An attractive avenue for producing doped large-area graphene thin films while altering their electronic band structure near the Dirac point in a limited way is through the use of metal NPs. This is particularly true in many cases where assembling metallic layers on top of graphene sheets is not viable for practical applications for which access to the graphene surface is required. **Figures 4a**, **b** and **c** from Akbari-Sharbaf *et al*. [5] show scanning electron micrographs (SEM) of Cu-NPs assembled on graphene-RNA-based films deposited by vacuum filtration followed by drying in a vacuum desiccator and annealing at 550°C for 5 h to remove RNA. Cu-NPs were deposited using RF sputtering of Cu metal target under high-vacuum conditions using very short sputter times to produce thin metal films, followed by annealing at temperatures ranging from 300–550°C for 1–4 h in a glove box under a nitrogen atmosphere. Annealing under an inert atmosphere was found to be an essential step in obtaining well-isolated Cu-NPs, while non-annealed Cu films formed a semi-continuous system of interconnected Cu particles. **Figures 4d** and **e** show how the average diameter of Cu-NPs and the fraction of graphene area covered can be controlled using the annealing temperature, while a longer annealing time promotes the formation of larger, more isolated NPs.

The work function of graphene-based films decorated with Cu-NPs was further investigated using scanning Kelvin probe force microscopy (SKPFM) shown in **Figure 5b** for a graphene substrate and **Figure 5e** for an ITO substrate. SKPFM is based on small electrostatic forces that are created between a conducting AFM tip and the sample when the two systems are in close proximity to determine the work function of a film. **Figures 5c** and **f** show the work function relative to Cu-NP size, indicating that the graphene-Cu work function decreases with increasing particle size with respect to bare graphene. Graphene-based films contain fewer free electrons compared to ITO, resulting in a larger work-function shift due to electron transfer from Cu-NPs.

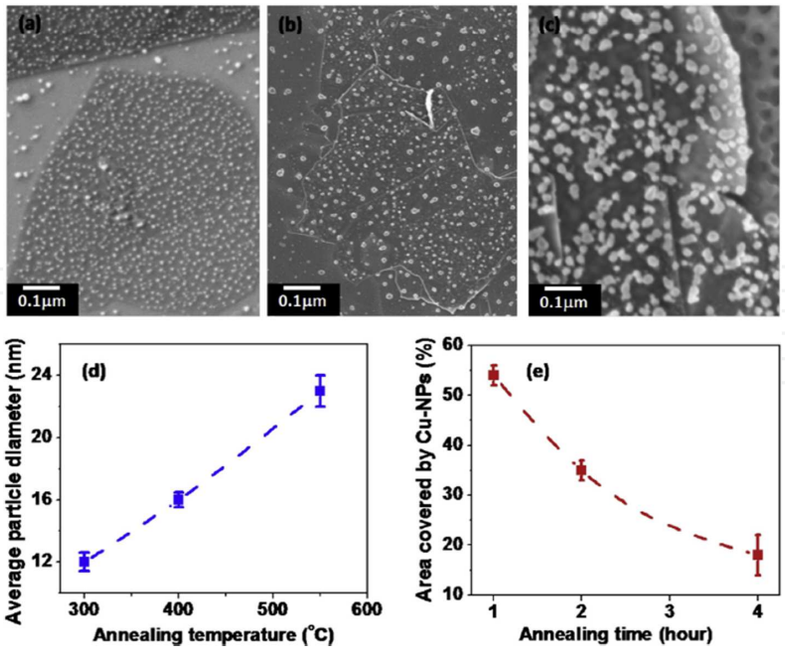

Figure 4. SEM images of graphene-based thin films decorated with Cu-NPs. Cu-NPs were deposited at different sputtering times of 2, 3, and 5 min, respectively, and annealed at (a) 300, (b) 400, and (c) 550°C. (d) Variation of the average diameter of Cu-NPs decorated on the graphene films shown in the SEM images. (e) Fraction of graphene surface covered by Cu-NPs. Reproduced with permission from Ref. [5].

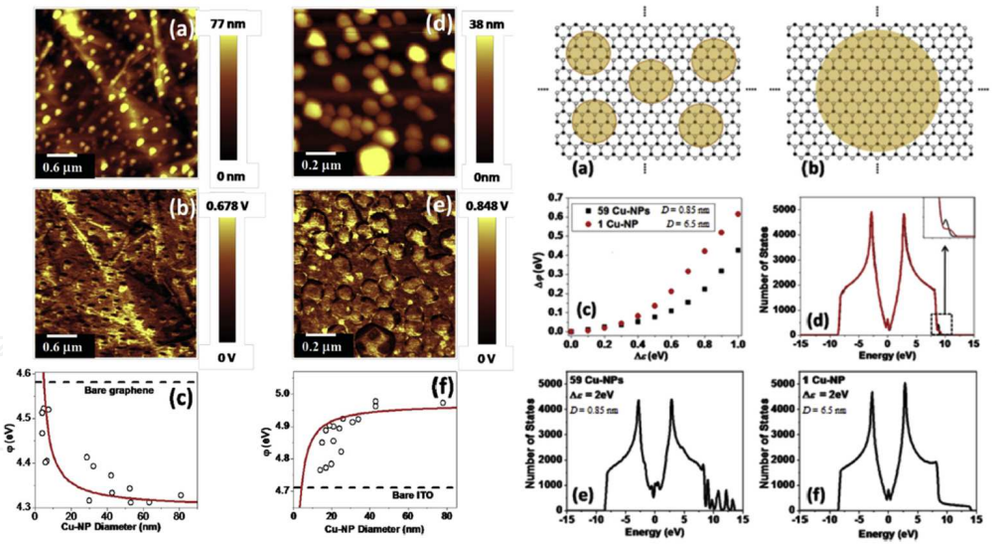

Figure 5. Left panel: (a) AFM and (b) SKPFM micrographs of graphene-based thin films decorated with Cu-NPs. (c) Plot of the work function vs. Cu-NP diameter. (d) AFM and (e) SKPFM micrographs of Cu-NPs on ITO. (f) Plot of the work function vs. Cu-NP diameter for Cu-NPs on ITO. **Right panel:** (a) 59 Cu-NPs of $D = 0.85$ nm diameter distributed randomly on a graphene lattice and (b) 1 Cu-NP of $D = 6.5$ nm. (c) Calculated shift in the work function. (d) The density of states for the two distributions indicated in panels a and b ($\Delta\varepsilon = 0.3$ eV). (e) and (f) show the density of states for the two distributions at $\Delta\varepsilon = 2$ eV. Reproduced with permission from Ref. [5].

The right panel of **Figure 5** describes the result of theoretical modeling of both the work function and the density of states (DOS) of graphene-based films decorated with either a random array of 59 small diameter Cu-NPs (0.85 nm) compared to a single large Cu-NP (6.5 nm). Graphene doping due to the Cu distribution can be well understood in the framework of a tight-binding model considering two different ionization energies, $\varepsilon_i = \varepsilon_0$ and $\varepsilon_j = \varepsilon_{mod}$, for two homogeneously distributed but non-equivalent carbon sites, *i* and *j*, interacting and non-interacting with Cu, respectively. The plot of the work-function shift as a function of the difference, $\Delta\varepsilon = \varepsilon_{mod} - \varepsilon_0$, of the local ionization energy of *i* and *j*-type carbon sites is reported in **Figure 5c** (right panel). For $\Delta\varepsilon > 0.3$ eV, the variations in work function change ($\Delta\varphi$) between the two systems are large, and shows that for stronger metal-carbon bonding the particle diameter plays a more significant role in shifting the work function away from the Dirac point of graphene, in addition to the major role played by the area fraction covered by metallic particles [5].

At small Δε, the DOS is only marginally different for the two distributions of Cu shown in the right panel of Figures 5a and b, as demonstrated by DOS plot in the right panel d. An important feature of the DOSs at high-energy differences between the Dirac point of graphene and the work function of metallic nanoparticles, shown in right panels e and f (Δε = 2 eV), shows the DOS is significantly affected by the particle size. If very small particles are randomly distributed on the graphene lattice, the DOS near the Fermi level is dramatically altered in its profile with the appearance of additional states, compared to pristine graphene (**Figure 5e** right panel). However, even at the largest values of Δε, the DOS profile near the Dirac point is preserved for large metallic nanoparticles, as demonstrated in right panel f for $D = 6.5$ nm. This suggests that for particles of $D > 10$ nm, the metal particle diameter plays a negligible role in determining the work-function shifts of graphene domains. These theoretical findings corroborate the SKPFM experiments, indicating that the Cu-NP diameter has only a moderate effect on the work-function shift (Δφ) of graphene where larger particles do not have a greater effect compared to smaller ones.

Strongly interacting metals such as Ni and Co have also been investigated for modifying graphene using metal nanoparticles. Ni has been shown to strongly interact with graphene surfaces and can be used to etch vacancies in graphene sheets or be used as an electrode material in graphene-based devices [1]. Cobalt nanoparticles on single-layer graphene have also been used for band engineering to open a small band gap in single-layer graphene at room temperature, sufficient for use in semiconducting applications [12]. In this application, both the size and the distribution of Co nanoparticles affects the band gap formation, which was controlled by using a very slow metal deposition rate (0.02 Å/s). A band gap is induced when the nanoparticle size is such that local oxidation is induced in the graphene by strong interaction with Co *d*-states and upon exposure to air, resulting in localization of free electrons in graphene at oxide sites and modification of the graphene band structure [12].

2.4. Specific properties and applications of graphene thin films decorated with arrays of metal nanoparticles

Graphene thin films decorated with random distributions of metallic nanoparticles have been shown to enhance optical and electronic properties, and new devices such as evanescent waveguides could emerge through self-assembling of nano-metallic phases into superlattices. Typically, expensive techniques such as nanolithography and nano-contact printing, suitable only over small areas, are required to attain nano-patterned structures on graphene or other 2D materials. For use over large areas, alternative methods have been proposed for the spontaneous self-assembly of metal nanoparticles such as Cu on graphene-based films. In the left panel of **Figure 6a** is shown a schematic of Cu-NP self-assembly on graphene-based films from Ouyang *et al*. [8]. Large-area, graphene-based films were deposited from a graphene-RNA dispersion discussed previously, followed by deposition of a Cu metal layer using thermal evaporation at very low deposition rates (0.5 nm/min). The left panel of **Figure 6c** shows the graphene immediately after Cu deposition, and **Figure 6d** shows the nucleation of Cu-NPs into a self-assembled superlattice.

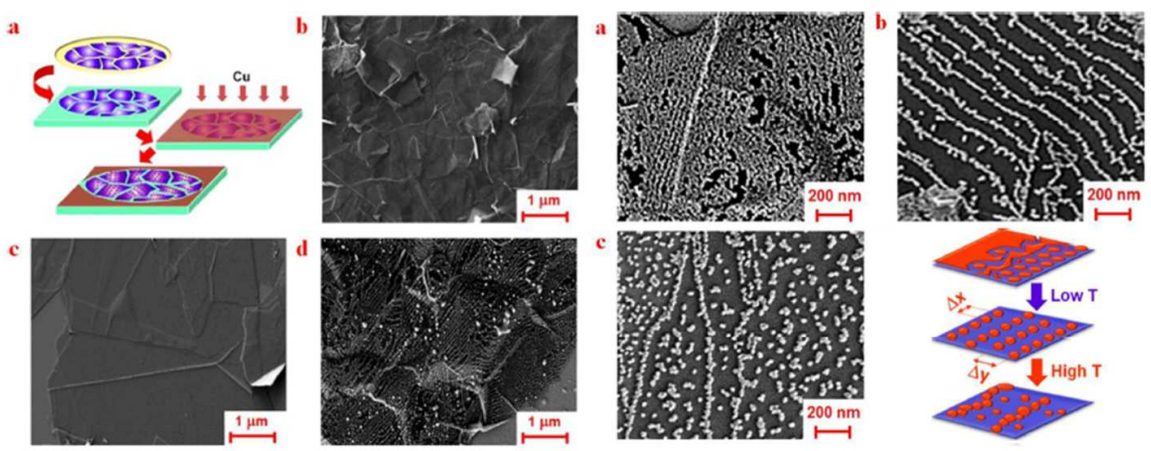

Figure 6. Left panel: (a) Fabrication of Cu-NPs superlattices: (i) deposition of a large-area graphene thin film; (ii) thermal evaporation of a 0.7 ± 0.3 nm-thick Cu layer, and (iii) thermal annealing of the system. (b) SEM of a bare graphene-based thin film on Si(100), (c) SEM of the same film after thermal evaporation of the Cu layer, and (d) SEM after thermal annealing. **Right panel**: SEM images of samples annealed for 8 h at increasing temperatures: (a) 200, (b) 360, and (c) 440°C. In the bottom right corner, a diagram shows the behavior of Cu-NP's nucleated at different temperatures. Reproduced with permission from Ref. [6].

The right panel of **Figure 6** shows the effect of different annealing temperatures that promote different conformations of Cu superlattices. The ideal annealing temperature was found to be 360°C, at which ordered superlattices of Cu-NPs with less than 20 nm diameter are created. After 8 h annealing at this temperature, Cu-NPs align in parallel lines along the armchair direction of the graphene lattice. The inter-particle spacing in this case is relatively low with a ~12 nm inter-particle spacing along the same line, while the spacing between lines is found to be one order of magnitude higher (~182 nm) [6]. The use of higher annealing temperatures' (**Figure 6**, right panel c) kinetic effects cause the Cu-NPs to become displaced from the superlattice structure observed at 360°C. At lower temperatures, shown in **Figure 6**, right

panels a and b, Cu-NP nucleation occurs when the thin Cu layer is in a molten state since the melting temperature of metallic nanoparticles and ultrathin metallic films of only a few atomic layers is significantly lower than in the bulk metal.

The propagation of evanescent waves along Cu-NP superlattices confined in the proximity of the graphene surface and propagating along the direction parallel to the Cu-NPs lines was investigated using three-dimensional scanning near-field optical microscope (3D-SNOM). In these experiments, a 532 nm laser is launched into a single-mode optical fiber and incident on the superlattice samples as shown in **Figure 7d** and **e**. SNOM (X,Z) scans were used to probe the decay of near-field evanescent modes moving away from the sample surface along the *z*-direction. Vertically, evanescent fields only exist within a distance equal to approximately one wavelength of incident light. In the near field, Cu-NPs display strong Mie scattering to $\lambda = 532$ nm light, and therefore the interaction between light and the Cu-Np superlattices is dominated by scattering [6]. Light incident on the Cu-Np superlattice experiences Mie scattering along a preferential direction when the interline distance (~100 nm) is the same order of magnitude as the wavelength of incident light. Light absorption occurs in the transverse direction to the NP lines, resulting in low attenuation for longitudinal modes and confinement of an evanescent wave as shown in **Figure 7d** [6].

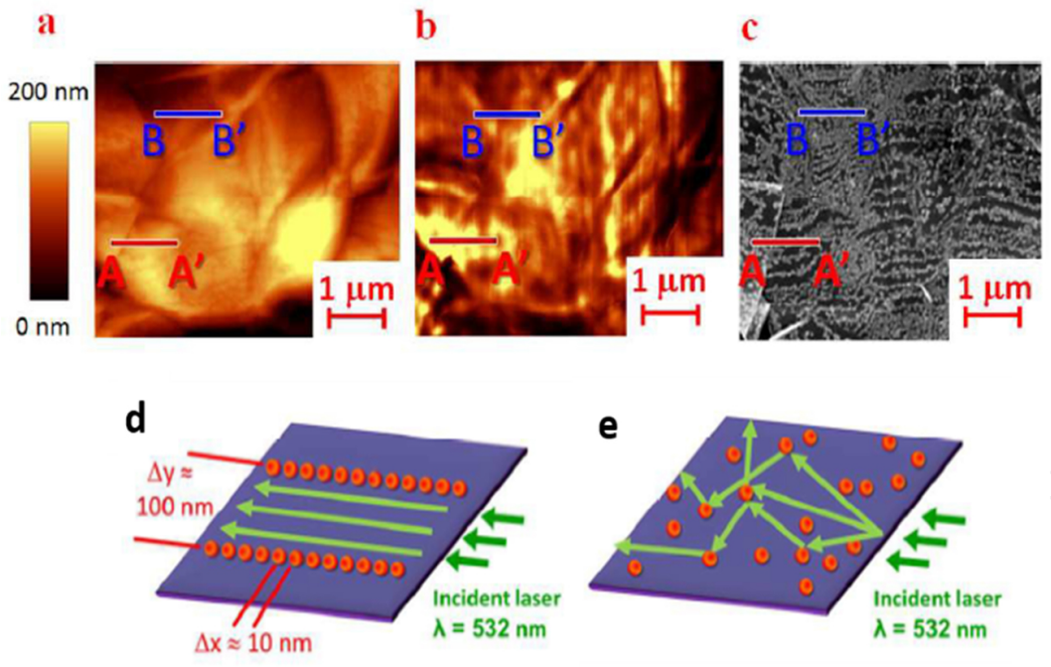

Figure 7. (a) AFM and (b) 3D-SNOM images obtained simultaneously from a Cu-NP superlattice annealed at 360°C for 8 h. (c) SEM micrograph obtained using lithographically patterned markers from the same sample region as in panels a and b. (d) Coherent scattering in superlattices and (e) incoherent scattering combined with light absorption in randomly distributed Cu-NPs. Reproduced with permission from Ref. [6].

Conversely, light will be isotropically scattered in all directions by randomly distributed Cu-NPs (**Figure 7e**), which causes interference between the far-field modes such that evanescent waves do not propagate. 3D-SNOM measurements in **Figure 7b** describe these two cases of

evanescent waveguide behavior in Cu-NPs superlattices (A-A′ region) and isotropic Mie scattering where Cu-NPs are disordered (B-B′ region). The area of the AFM topography shown in **Figure 7a** is the same area defined in the SNOM image of **Figure 7b**, in which a brighter pixel represents a higher intensity of scattered light being collected at that point in close proximity to the sample at low *z* distances.

Figures 7b and **c** show a superlattice of Cu-NP's aligned parallel to the light propagation direction which is along the Y-axis. The SEM of **Figure 7c** shows that the Cu-NP distribution is ordered in the A-A′ region, and significantly less ordered in the region B-B′. From this result, the section A-A′ is expected to function as an evanescent waveguide, while B-B′ should exhibit a sequence of constructive and destructive interference patterns along the vertical axis, due to Mie scattering [6]. Along the A-A′ section, confinement of the electromagnetic radiation in the bright yellow zone in the proximity of the sample surface can be observed. A strong attenuation of light intensity at values of *Z* (not shown) within a few tens of nanometers from the sample surface was also observed, verifying the presence of evanescent modes in the A-A′ region.

3. Conclusions

Graphene and graphene-based films can be fabricated using a variety of methods including vacuum deposition techniques such as CVD, to solution-based techniques focusing on the exfoliation of graphite in aqueous solutions. CVD techniques are typically used to produce pristine grains of single- and few-layer graphene grown on Ni and Cu substrates. Graphene of this type is high quality, but can be costly to produce and requires an additional process often based on a sacrificial polymer layer to transfer the graphene to other substrates for device applications. Although the as-prepared graphene samples are of high quality, defects and contamination can be introduced during the transfer process, lowering the overall quality of the final product. Graphene-based materials produced from chemical exfoliation of graphite can overcome some issues with vacuum techniques where chemical exfoliation does not require vacuum facilities and is suitable to scaling up to large quantities. Graphene and graphene oxide dispersions in water obtained by oxidation or the use of a surfactant can be used to produce graphene-based films using simple deposition techniques such as vacuum filtration or spin coating. Although more suitable for large-scale production, chemical exfoliation methods may be less reproducible as the quality of the final graphene-based film depends strongly on the specific fabrication parameters.

It has been shown that films produced from interlocking and overlapping graphene platelets have optical, electrical, and thermal properties that diverge from single-layer graphene. These films may therefore be more desirable for various electronic and device applications, particularly if they are further modified with metal nanoparticles. In this application, the deposition and nucleation conditions of metal NPs determine the properties of the resulting graphene-NP films. The nucleation of metal NPs and their size can be controlled using slow metal deposition rates combined with long annealing times at relatively low temperatures in an inert atmosphere to avoid metal oxidation. These techniques can be used to obtain self-assembled

arrays of NPs on graphene-based films that can be used in new types of nano-devices such as evanescent waveguides. It is clear that metal NP modified graphene materials are well positioned as new materials with enhanced properties to be used in the next generation of electronic devices.

Acknowledgements

PB acknowledges a MITACS Accelerate Postdoctoral Fellowship. AAS acknowledges an Ontario MRI Queen Elizabeth II Graduate Scholarship. JP acknowledges a Nanofabrication Facility Graduate Student Award from the University of Western Ontario. GF acknowledges a Canada Research Chair in carbon-based nanomaterials. The authors would like to thank Dr. M.S. Ahmed, Dr. R.J. Bauld, Dr. F. Sharifi, and Mr. A. Venter for some of the experiments that led to the results discussed here, and for fruitful discussions. Funding from the Canada Foundation for Innovation (grant no. 212442) and the Discovery Grant program of the Natural Sciences and Engineering Research Council of Canada (RGPIN-2015-06004) are also gratefully acknowledged.

Author details

Paul Bazylewski[1], Arash Akbari-Sharbaf[1], Sabastine Ezugwu[1], Tianhao Ouyang[1], Jaewoo Park[1] and Giovanni Fanchini[1,2*]

*Address all correspondence to: gfanchin@uwo.ca

1 Department of Physics and Astronomy, University of Western Ontario, London, Canada

2 Department of Chemistry, University of Western Ontario, London, Canada

References

[1] Zhang Y, Zhang L, Zhou C. Review of chemical vapor deposition of graphene and related applications. Accounts of Chemical Research. 2013;46:2329–2339. DOI: 10.1021/ar300203n

[2] Park S, Ruoff RS. Chemical methods for the production of graphenes. Nature Nanotechnology. 2009;5:309–309. DOI: 10.1038/nnano.2009.58

[3] Zhu Y, Murali S, Cai W, Li X, Suk JW, Potts JR, Ruoff RS. Graphene and graphene oxide: synthesis, properties, and applications. Advanced Materials. 2010;22:3906–3924. DOI: 10.1002/adma.201001068

[4] Sharifi F, Bauld R, Ahmed MS, Fanchini G. Transparent and conducting graphene-RNA-based nanocomposites. Small. 2012;8:699–706. DOI: 10.1002/smll.201101537

[5] Akbari-Sharbaf A, Ezugwu S, Ahmed MS, Cottam MG, Fanchini G. Doping graphene thin films with metallic nanoparticles: experiment and theory. Carbon. 2015;95:199–207. DOI:10.1016/j.carbon.2015.08.021

[6] Ouyang T, Akbari-Sharbaf A, Park J, Bauld R, Cottam MG, Fanchini G. Self-assembled metallic nanoparticle superlattices on large-area graphene thin films: growth and evanescent waveguiding properties. RSC Advances. 2015;5:98814–98821. DOI: 10.1039/c5ra22052a

[7] Ahmed MS, Ezugwu S, Divigalpitiya R, Fanchini G. Relationship between electrical and thermal conductivity in graphene-based transparent and conducting thin films. Carbon. 2013;61:595–601. DOI:10.1016/j.carbon.2013.05.041

[8] Bauld R, Ahmed MS, Fanchini G. Optoelectronic and thermal properties of solution-based graphene thin films. Physica Status Solidi C. 2012;9:2374–2379. DOI: 10.1002/pssc.201200292

[9] Bauld R, Sharifi F, Fanchini G. Solution processed graphene thin films and their applications in organic solar cells. International Journal of Modern Physics B, 2012;26:1242004. DOI: 10.1142/S0217979212420040

[10] Venter A, Hesari M, Ahmed MS, Bauld R, Workentin MS, Fanchini G. Facile nucleation of gold nanoparticles on graphene-based thin films from Au144 molecular precursors. Nanotechnology. 2014;25:135601. DOI:10.1088/0957-4484/25/13/135601

[11] Bauld R, Hesari M, Workentin MS, Fanchini G. Thermal stability of Au_{25} molecular precursors and nucleation of gold nanoparticles in thermosetting polyimide thin films. Applied Physics Letters. 2013;101:243114. http://dx.doi.org/10.1063/1.4770515

[12] Bazylewski PF, Nguyen VL, Bauer RPC, Hunt AH, McDermott EJG, Leedahl BD, Kukharenko AI, Cholakh SO, Kurmaev EZ, Blaha P, Moewes A, Lee YH, Chang GS. Selective area band engineering of graphene using cobalt-mediated oxidation. Scientific Reports. 2015;5:15380. doi:10.1038/srep15380